A1 R HD25

High-Definition Resonant Scanning Confocal System

More Data, Faster

- Largest field of view on the market
- Acquire 2x the amount of data per scan
- Acquire larger fields of view without compromising resolution
- Long working distance optics for imaging organoids and organ-chips

Stunning High-Definition Images at Resonant Speed

- Acquire 1024 x 1024 high-definition images at high-speed
- AI-based noise removal from resonant scanned images

Powerful Acquisition and Analysis Tools

- Fully customizable acquisition and analysis workflows
- AI-enabled tools for image processing and analysis

www.microscope.healthcare.nikon.com/a1rhd25

Nikon Instruments Inc. • nikoninstruments.us@nikon.com • 1-800-52-NIKON

Received: 15 September 2020 | Revised: 28 November 2020 | Accepted: 22 December 2020

DOI: 10.1002/jcp.30256

RESEARCH ARTICLE

Journal of Cellular Physiology WILEY

Osteoprotegerin is sensitive to actomyosin tension in human periodontal ligament fibroblasts

Andrew C. Tamashunas[1] | Aditya Katiyar[2] | Qiao Zhang[1] | Purboja Purkayastha[3] | Pankaj K. Singh[4,5] | Sasanka S. Chukkapalli[6,7] | Tanmay P. Lele[2,3,8]

[1]Department of Chemical Engineering, University of Florida, Gainesville, Florida, USA

[2]Department of Biomedical Engineering, Texas A&M University, College Station, Texas, USA

[3]Artie McFerrin Department of Chemical Engineering, Texas A&M University, College Station, Texas, USA

[4]GCC Center for Advanced Microscopy and Image Informatics, Houston, Texas, USA

[5]Center for Translational Cancer Research, Texas A&M University, Houston, Texas, USA

[6]Department of Oral Biology, College of Dentistry, University of Florida, Gainesville, Florida, USA

[7]Center for Molecular Microbiology, University of Florida, Gainesville, Florida, USA

[8]Department of Translational Medical Sciences, Texas A&M University, College Station, Texas, USA

Correspondence

Sasanka S. Chukkapalli, Department of Oral Biology and Center for Molecular Microbiology, College of Dentistry, University of Florida, Gainesville, FL 32611, USA.
Email: schukkapalli@dental.ufl.edu

Tanmay P. Lele, Department of Biomedical Engineering, Texas A&M University, College Station, TX 77840, USA.
Email: tanmay.lele@tamu.edu

Abstract

Periodontal ligament fibroblasts (PdLFs) are an elongated cell type in the periodontium with matrix and bone regulatory functions which become abnormal in periodontal disease (PD). Here we found that the normally elongated and oriented PdLF nucleus becomes rounded and loses orientation in a mouse model of PD. Using in vitro micropatterning of cultured primary PdLF cell shape, we show that PdLF elongation correlates with nuclear elongation and the presence of thicker, contractile F-actin fibers. The rounded nuclei in mouse PD models in vivo are, therefore, indicative of reduced actomyosin tension. Inhibiting actomyosin contractility by inhibiting myosin light chain kinase, Rho kinase or myosin ATPase activity, in cultured PdLFs each consistently reduced messenger RNA levels of bone regulatory protein osteoprotegerin (OPG). Infection of cultured PdLFs with two different types of periodontal bacteria (*Porphyromonas gingivalis* and *Fusobacterium nucleatum*) failed to recapitulate the observed nuclear rounding in vivo, upregulated nonmuscle myosin II phosphorylation and downregulated OPG. Collectively, our results add support to the hypothesis that PdLF contractility becomes decreased and contributes to disease progression in PD.

KEYWORDS

F-actin fibers, mechanobiology, mechanotransduction, nucleus, osteoprotegerin, periodontal disease, periodontal ligament fibroblasts

1 | INTRODUCTION

The periodontal ligament (PDL) is a fibrous, soft connective tissue that attaches the cementum of the tooth to the alveolar bone (Figure 1a). The PDL is part of the dynamic periodontal complex in which the magnitude and frequency of mechanical forces generated through processes such as chewing control regulatory functions of bone, cementum and the ligament (Jang et al., 2018; Lee et al., 2015). These forces modulate biochemical pathways in cells in the periodontium through mechanisms that are not fully understood.

The periodontal ligament fibroblast (PdLF) is an elongated cell type in the PDL that has important matrix remodeling and signaling functions in the PDL. PdLFs secrete extracellular proteins like collagen and organize them into fibers (Berkovitz, 1990). They also secrete matrix metalloproteinases (Assis Lisboa et al., 2009; Liu et al., 2012; Ziegler et al., 2010) that remodel the extracellular matrix. PdLFs

Andrew C. Tamashunas and Aditya Katiyar contributed equally.

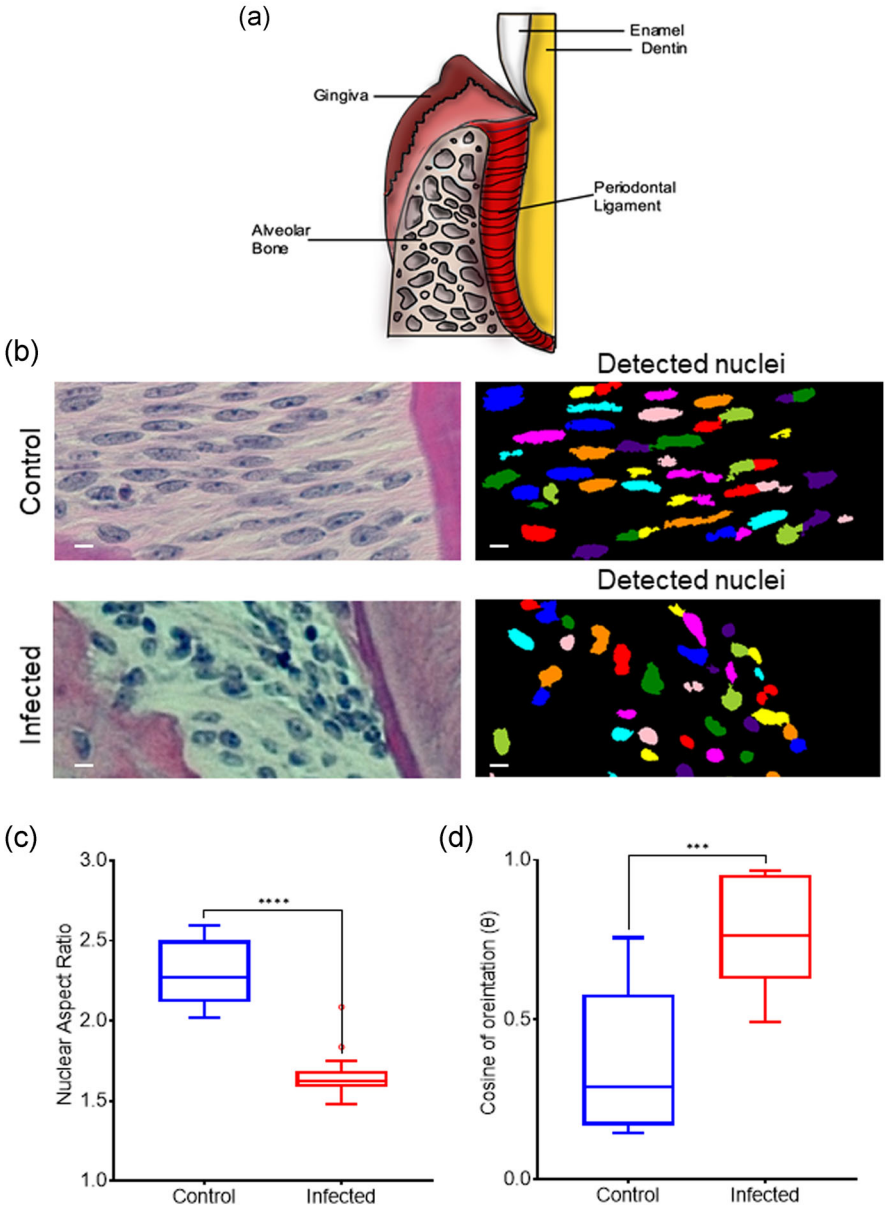

FIGURE 1 Effect of periodontal disease on nuclear morphology and orientation. (a) Schematic of the periodontium consisting of alveolar bone, gingiva, tooth, and periodontal ligament. (b) Representative images of regions of the region between bone and cementum in control and bacterial infected mice, and nuclei segmented using computational methods. Mice were infected with bacteria for a period of 16 weeks (see Section 2). Control mice were sham infected with vehicle. (c) Quantification of nuclear aspect ratio (long axis/short axis). "****" Represents statistically significant difference by Mann–Whitney test ($p < .0001$). Scale bar is 20 μm. (d) Cosine of the angle θ between the vertical line and the major axis of the ellipse, which is a measure of orientation. Data corresponds to 9 control and 14 infected images from six mice per condition (575 nuclei quantified in control and 781 nuclei in infection). "****" Represents statistically significant difference by Mann–Whitney test ($p = .0005$)

express proteins that have a key role in controlling alveolar bone remodeling (McCulloch et al., 2000). Mechanical modulation of bone regulatory gene expression in PdLFs by tensile or compressive stresses in the PDL is thought to ensure interdigitation of teeth through resorption and formation of maxillary and mandibular bones. For example, tensile stress upregulates osteoprotegerin (OPG) in PdLFs (Tsuji et al., 2004). Conversely, compressive orthodontic force upregulates the osteoclastogenic receptor activator NF kappa B ligand (RANKL) in PdLFs in vivo (Kim et al., 2007).

The periodontium hosts a diverse range of nearly 600 types of oral bacteria (Moore & Moore 1994; Socransky & Haffajee, 2005), which continually initiate an inflammatory cascade in the periodontal tissue environment (Cekici et al., 2014). When a subset of these bacteria become dominant, causing dysbiosis or a loss of equilibrium, chronic periodontal disease can be a result (Lamont & Hajishengallis, 2015; Marsh, 2015; Roberts & Darveau, 2015). Dysbiosis causes a progressive resorption of alveolar bone and ultimately a loss of teeth (Jiao et al., 2014; Pihlstrom et al., 2005). PdLFs maintain the bone equilibrium under

normal physiological conditions through a balance of OPG/RANKL levels but this equilibrium is tilted towards osteoclastogenesis during pathological conditions of periodontal disease (PD; Binderman et al., 2002; El-Awady et al., 2010b; Sokos et al., 2015b).

Despite the fact that mechanical control of gene expression critically determines the bone-regulatory functions of the periodontal complex, how mechanical forces regulate bone regulatory gene expression in PdLFs (reviewed in Chukkapalli & Lele, 2018) and how these relationships become abnormal in PD is not fully understood. It is known from other model systems and in vivo studies that the contractile actomyosin cytoskeleton plays an important role in transduction of external mechanical forces into changes in intracellular pathways (Chicurel et al., 1998; Lee & Kumar, 2016; Mammoto et al., 2013). Organized partly into discrete fibers, the actomyosin cytoskeleton continuously generates internal cytoskeletal tension which is transmitted to the extracellular matrix at cell-matrix adhesions (Balaban et al., 2001; Lele et al., 2006; Prager-Khoutorsky et al., 2011). Actomyosin fibers which contain nonmuscle myosin II (NMMII), and generate tension through NMMII motor action along F-actin filaments (Kassianidou & Kumar, 2015; Lee & Kumar, 2016). Such tension generation can be experimentally observed through the retraction of laser-severed actomyosin fiber ends in cells (Kassianidou & Kumar, 2015; Kumar et al., 2006; Lee & Kumar, 2016; Russell et al., 2009; Stachowiak & O'Shaughnessy, 2009). NMMII-based tension generated by actomyosin fibers is essential for wound healing by fibroblasts and is physiologically important (Goffin et al., 2006; Tomasek et al., 2013; Wipff et al., 2007). Given that compressive stress, which should cause a decrease in actomyosin contractility in cells, upregulates alveolar bone resorptive functions of PdLFs in vivo (Kim et al., 2007), and that alveolar bone becomes resorbed in PD, it is reasonable to suppose that actomyosin tension in PdLFs may be reduced in PD which may in turn modulate bone regulatory gene expression. Therefore, in this study, we examined the effect of inhibiting actomyosin tension on messenger RNA (mRNA) levels of putative mechanosensitive genes in PdLFs.

2 | METHODS

2.1 | Bacterial growth conditions

Porphyromonas gingivalis strain W83 and *Fusobacterium nucleatum vincentii* strain 49256 (both from American Type Culture Collection) were grown as previously described under anaerobic conditions at 37°C in an atmosphere of 10% H_2, 5% CO_2 and 85% N_2 (Chukkapalli et al., 2015). *P. gingivalis* W83 were cultured on blood agar plates supplemented with hemin (5 μg/ml) and VitK1 (1 μg/ml) or tryptic soy broth (TSB) media supplemented with hemin (5 μg/ml) and vitamin K1 (1 μg/ml). *F. nucleatum* were cultured on blood agar plates supplemented with hemin (5 μg/ml) and vitamin K1 (1ug/ml) or brain heart infusion (BHI) broth. Bacteria were grown in their respective culture medium until their logarithmic growth phase (growth rate was measured from plots of optical density [OD_{550nm}] vs. time). Inocula for infection were prepared by dilution of the appropriate volume of TSB/BHI culture in antibiotic free SCGM media to achieve a multiplicity of infection (MOI) of 100. Culture purity and morphological characteristics of each bacterium used for infection experiments were assessed by gram stains for all cultures prepared in this study.

2.2 | In vivo mouse studies

C57BL6/J mice were purchased from the Jackson Laboratory (The Jackson Laboratories) and housed in microisolator cages in a pathogen free environment. All the experimental protocols were approved by the Institutional Animal Care and Use Committee, University of Florida (approval no.: 201710038). Mice were randomly divided in to two groups, (i) infection group and (ii) control group ($n = 6$ in each group). Mice were infected orally with a mixture of periodontal bacterial flora *P. gingivalis* and *F. nucleatum* (1×10^9 cfu/ml; Chukkapalli et al., 2015). Infection was done three times per week every other week for 16 weeks corresponding to a total of 24 infections. Control mice were identically sham-infected with sterile vehicle (carboxymethyl cellulose). After the infection period, animals were euthanized and mandible specimens collected, immersion fixed in 4% paraformaldehyde followed by processing for paraffin sectioning as previously described (Chukkapalli et al., 2015). The specimens were sectioned (4 μm) in the mesio-distal direction and stained with hematoxylin and eosin (H&E). Histological images were captured and scanned using ScanScope CS system (Aperio). Image viewing was done at ×200 magnification using ImageScope viewing software (Aperio). PdLFs were identified in the periodontal ligament by their location and this region of interest was further used for the quantitative analysis in Figure 1.

2.3 | Nuclear segmentation and image analysis

Ilastik was used to segment the nuclei from the images. Holes were filled in the segmented images and small objects with less than 100 pixels were removed. Using a watershed algorithm, touching nuclei were separated when possible. For each detected nucleus, we compute two features, namely, the aspect ratio (ratio of major and minor axes of the smallest ellipse enclosing the nucleus), and the cosine of its orientation. For each sample, the median values of these features were obtained. Mann–Whitney test was performed to evaluate statistically significant differences in the median aspect ratio as well as for the median of cosine of the orientation.

2.4 | PdLF culture and growth conditions

Primary human PdLFs were obtained from Lonza (Catalog: #CC-7049). PdLFs were grown in SCGM growth medium (Catalog: #CC-3205; Lonza) as per the manufacturer's instructions at 37°C in a humidified 5% CO_2 atmosphere. After reaching 70%–80% confluence, cells of the fourth passage were passaged using trypsin/EDTA (Invitrogen) and were used for experiments at fifth passage.

2.5 | Microcontact printing

For creating fibronectin patterns, hydrophilic polymer tissue culture dishes (Catalog: #80136; Ibidi) were stamped with rhodamine-conjugated fibronectin (Catalog: #FNR01; Cytoskeleton Inc.) in 1-D lines 75 μm or 300 μm in length and 5 μm in width with by microcontact printing as previously described (Thery & Piel, 2009). Briefly, a silicon wafer was etched with surface features using standard photolithography techniques. Then, polydimethylsiloxane (Catalog: #DC4019862; Sylgard 184 Silicone Elastometer Kit; Dow Corning) was mixed at manufacturer's recommended base to curing agent ratio of 10:1 (wt/wt) and cured at 60°C in a convection oven for 2 h against the silicon wafer. The PDMS stamp was then peeled off and cut to required shape and size. Rhodamine-conjugated fibronectin (Catalog: #FNR01; Cytoskeleton Inc.) was diluted to 20 μg/ml in DI water and a 20 μl drop was adsorbed onto the stamp surface for 1 h. Culture dishes were treated for 2 min with low-frequency plasma cleaner unit (PE-25; PlasmaEtch Inc.) before contact printing them with the rinsed and dried stamps. Nonprinted regions of the dish were passivated with 0.2 mg/ml PLL-g-PEG solution (Surface Solutions) for 1 h to prevent inadvertent protein adsorption and cell adhesion on nonprinted regions.

2.6 | Immunostaining

PdLFs were fixed in 4% paraformaldehyde (Catalog: #J61899; Alfa Aesar) at room temperature for 10 min, washed three times with 1X phosphate-buffered saline (PBS; Catalog: #21-040-CM; Corning), and pretreated with permeabilization buffer (0.1% Triton-X, 1% bovine serum albumin and PBS) for 2 h. Samples were washed three times with PBS post-permeabilization and incubated overnight at 4°C with monoclonal mouse anti-vinculin (Catalog: #ab130007; Abcam) and/or monoclonal rabbit antiphosphorylated myosin with light chain (s20) antibody (Catalog: #ab2480; Abcam) diluted in PBS as per manufacturer's recommendation. After this, samples were washed three times with PBS and incubated with Alexa Fluor 594 goat anti-rabbit antibody (Catalog: #A-11037; Invitrogen) and/or Alexa Fluor 647 donkey anti-mouse antibody (Catalog: #A-31571; Invitrogen). Hoechst (Catalog: #875756-97-1, H33342; Sigma-Aldrich) was used to stain DNA. Alexa Fluor-488 phalloidin (A12379; Thermo Fisher Scientific) was used to stain F-actin.

2.7 | Microscopy

Fixed and stained samples were mounted in glycerol-based aqueous mounting medium (Catalog: #H-1000; Vectashield; Vector Labs) against a No.1.5 glass coverslip before imaging.

Imaging was performed on a Nikon Ti2 eclipse laser scanning A1 confocal microscope (Nikon) with a Nikon CFI Plan Apo Lambda 60X/1.4 NA oil immersion objective lens (MRD01605). Immersion oil Type 37 (Catalog: #16237; Cargille Labs) was used at 37°C (R.I. = 1.5238 for $\lambda = 486.1$ nm). A pinhole opening of 1 Airy disk was selected and the images were acquired at a resolution of 512 by 512 pixels.

Heat maps in insets that show colocalization of phosphorylated regulatory myosin light chain (pMLC)-II or vinculin with F-actin were generated using built in colocalization LUT function in FIJI. Black/dark blue regions represent absence of both F-actin and pMLC-II/vinculin whereas presence of either f-actin or pMLC-II/vinculin is represented by royal blue pixels. Magenta represents colocalization of F-actin with pMLC-II/vinculin and strong colocalizations were represented by a pixel color shift towards yellow/white.

2.8 | Western blotting

For assaying pMLC levels, PdLF cells were washed with cold PBS and lysed in lysis buffer (50 mM Tris-HCl pH 7.2, 1% (wt/vol) Triton X-100, 500 mM NaCl, 10 mM $MgCl_2$, and 0.1% vol/vol sodium dodecyl sulfate) supplemented with 1% vol/vol protease inhibitor (Cytoskeleton Inc.) on ice. Cells were then scraped from the dish and centrifuged at 10,000 rpm (Eppendorf, 5415 R) for 5 min at 4°C. The supernatant was collected, snap-frozen in liquid nitrogen, and stored at −80°C. Total protein concentrations were determined using Precision Red advance protein kit (Cytoskeleton Inc.). Levels of pMLC were quantified using the WES system (Protein Simple) and the 12–230 kDa simple WES kit (SM-W004), according to manufacturer's instructions; the antibody for pMLC was the same as in the immunostaining experiments above; glyceraldehyde 3-phosphate dehydrogenase (GAPDH) was blotted with monoclonal rabbit antibody (Catalog: #5174S; Cell Signaling Technology).

2.9 | Real time quantitative polymerase chain reaction

PdLFs were cultured in 96-well plate wells (round bottom) and treated with myosin inhibitors for 24 h without media change or re-supplementation. Cells that were labelled as vehicle control group were treated with only dimethyl sulfoxide (DMSO; 0.9% DMSO) while the rest of the groups were treated with ML-7: 25 μM, Y-27632: 25 μM, Blebbistatin: 50 μM for 24 h, respectively.

After the treatment period, cells were lysed and gene expression was assayed using respective probe-based real time-quantitative polymerase chain reaction (RT-qPCR). Quantitative PCR (qPCR) was performed using Taqman primers and probes on a QuantStudio 12K Flex Real-Time PCR System (Applied Biosystems/Life Technologies). Control qPCR reactions included substitution of No template RT and nuclease free water only, in place of primers and template, to ensure specific amplification in all assays. Dissociation curves for primer sets were evaluated to ensure that no amplicon-dependent amplification occurred. Data generated by qPCR were analyzed to first calculate using ΔCt values calculate as the difference between Ct value of GAPDH and the Ct value of the gene of interest for a given sample. Next, ΔΔCt was calculated as the difference between the ΔCt value of a given gene in cells treated with an inhibitor and the ΔCt value of that gene in DMSO treated cells. The ΔΔCt values, which are the log fold-change in mRNA levels relative to the DMSO control, were plotted in the figures. The standard error of the mean for ΔΔCt was calculated through error propagation as the square root of the

sum of the squares of ΔCt values of treatment and control. All statistical comparisons were performed on ΔCt values and significant differences were indicated on the ΔΔCt plots.

For cytokine treatment, PdLFs were seeded at 80,000 cells/well in a 96-well plate and incubated for 24 h before treatment. Later cells were treated with tumor necrosis factor-alpha (TNF-α; 5 ng/ml), transforming growth factor beta (TGF-β; 5 ng/ml) for 24 h, respectively (Hyun et al., 2017; Konermann et al., 2012; Luo et al., 2014; Palioto et al., 2011) and subject to PCR analysis.

3 | RESULTS

3.1 | Loss of elongated nuclear shapes during periodontal disease in vivo

It has been proposed that relaxation of tension in cells adherent to collagen bundles in the periodontium may promote alveolar bone resorption (Binderman et al., 2002, 2014). Because the degree of cell elongation is strongly correlated with actomyosin tension in cells (Bruyère et al., 2019), we hypothesized that cells in the PDL will be substantially rounded in infected periodontal tissue relative to control tissue. We therefore sought to quantify cell elongation using a mouse model of PD that we have previously developed (Chukkapalli et al., 2016). Mice were infected orally with a mixture of periodontal bacterial flora *P. gingivalis* and *F. nucleatum*. Control mice were simultaneously sham-infected with sterile vehicle (carboxymethyl cellulose). After the infection period, animals were euthanized and mandible specimens collected and imaged as previously described (Chukkapalli et al., 2016; see Section 2). Histological images were analyzed using image processing algorithms (see Section 2). As the highly elongated cells proved difficult to segment in H&E images of the region between the cementum and the periodontium (Figure 1b), and because the degree of nuclear elongation correlates directly with cell elongation (Katiyar et al., 2019; Lele et al., 2018), we chose to instead quantify nuclear elongation as a quantitative and simple measure of cell elongation in the tissue.

Nuclei in control H&E images in control regions between the cementum and the alveolar bone were elongated and oriented roughly perpendicular to the cementum (Figure 1b). In contrast, nuclear shapes were rounded with a loss of orientation in PD. The aspect ratio, a measure of elongation, was significantly lower in infected images compared to control images (Figure 1c). Likewise, the cosine of the orientation angle of the nucleus (Figure 1d) is significantly different between control images and infected images. The observed nuclear rounding and loss of orientation likely reflects rounding of cell shape, which in turn is suggestive of a decrease in actomyosin tension. We next asked how contractile actomyosin fibers, which generate tension in many cell types in vivo and in vitro, are impacted by PDLF cell shape in vitro.

3.2 | Effect of cell elongation on F-actin fiber assembly

We first investigated whether contractile F-actin fibers are present in primary human PdLFs in culture. Cultured PdLFs assembled clear F-actin labeled fibers (Figure 2a). However, not all F-actin fibers are contractile in cells, that is, not all F-actin fibers generate tension. We therefore sought to identify tension-generating or contractile fibers in PDLFs. Contractile F-actin fibers contain pMLC (Beach et al., 2014). Antibody labeling of pMLC revealed that pMLC colocalized with long F-actin fibers primarily along the cell periphery (Figure 2a and yellow arrows in Figure 2b). PdLFs also assembled non-pMLC containing F-actin fibers (Figure 2a and green arrows in Figure 2b) which tended to be in cell protrusions. These results suggest that long fibers at the PdLF periphery tend to be contractile, while fibers in protrusions tend to be not contractile. We also confirmed that contractile actin fibers terminated in vinculin labeled focal adhesions at either end while noncontractile fibers terminated in adhesions only at one end (Figures S1 and S2).

Given our in vivo results in Figure 1, we asked how cell elongation affects the spatial distribution of F-actin fibers in PdLFs. We micropatterned PdLFs on 1-D fibronectin lines which had a thickness of 5 microns. Areas outside the fibronectin line were passivated against matrix protein adsorption to prevent adhesion of cells outside of the lines. Elongated PdLFs on 1-D lines contained elongated nuclei, and also clearly defined peripheral F-actin fibers (marked by yellow arrows in Figure 2c). Micropatterning PdLFs on short fibronectin lines which constrained the degree of elongation of the cell resulted in cells featuring protrusions at one or both ends (Figure 2d). The fibers in these protrusions tended to be short in contrast (green arrowheads), and any peripheral fibers tended to be short and thin in comparison to those in elongated cells (yellow arrowheads in Figure 2d). Also, the nucleus in these cells tended to be rounded compared to nuclei in elongated fibroblasts (Figure 2e). This supports our assumption related to Figure 1 that cell elongation correlates with nuclear elongation. Collectively, the in vivo and in vitro studies suggest that rounding of PdLF cell shapes *in vivo* likely is concomitant with a decrease in the proportion of intracellular F-actin fibers that are contractile. This is consistent with other studies in different cell types which have shown that cell rounding results in decreased overall cell tension (Chen et al., 2003; Ingber et al., 1995; Polte et al., 2004).

3.3 | Myosin activity is a potent regulator of OPG

We next set out to inhibit actomyosin contractility in PdLFs and examined the effect of such modulation on mRNA levels of a few chosen genes. MLC phosphorylation is regulated by two different enzymes—Rho-associated kinase (ROCK) which is an effector of Rho GTPase, and myosin light chain kinase (MLCK) whose activation mechanism involves a calcium dependent calmodulin pathway (Katoh et al., 2001; Ridley & Hall, 1992, 1994; Tanner et al., 2010). We sought to inhibit myosin activity by using three different inhibitors: ML-7 which is an inhibitor of MLCK, Y27632 which is an inhibitor of ROCK, and blebbistatin, a specific myosin ATPase inhibitor. Treatment of cells with these drugs appeared to alter F-actin fiber numbers and/or distribution (Figure 3a) as reported by others (Tanner et al., 2010).

We examined the effect of pharmacological modulators of NMMII on the mRNA levels of key genes that are important in periodontal disease. The main criterion for choosing the assayed genes was prior

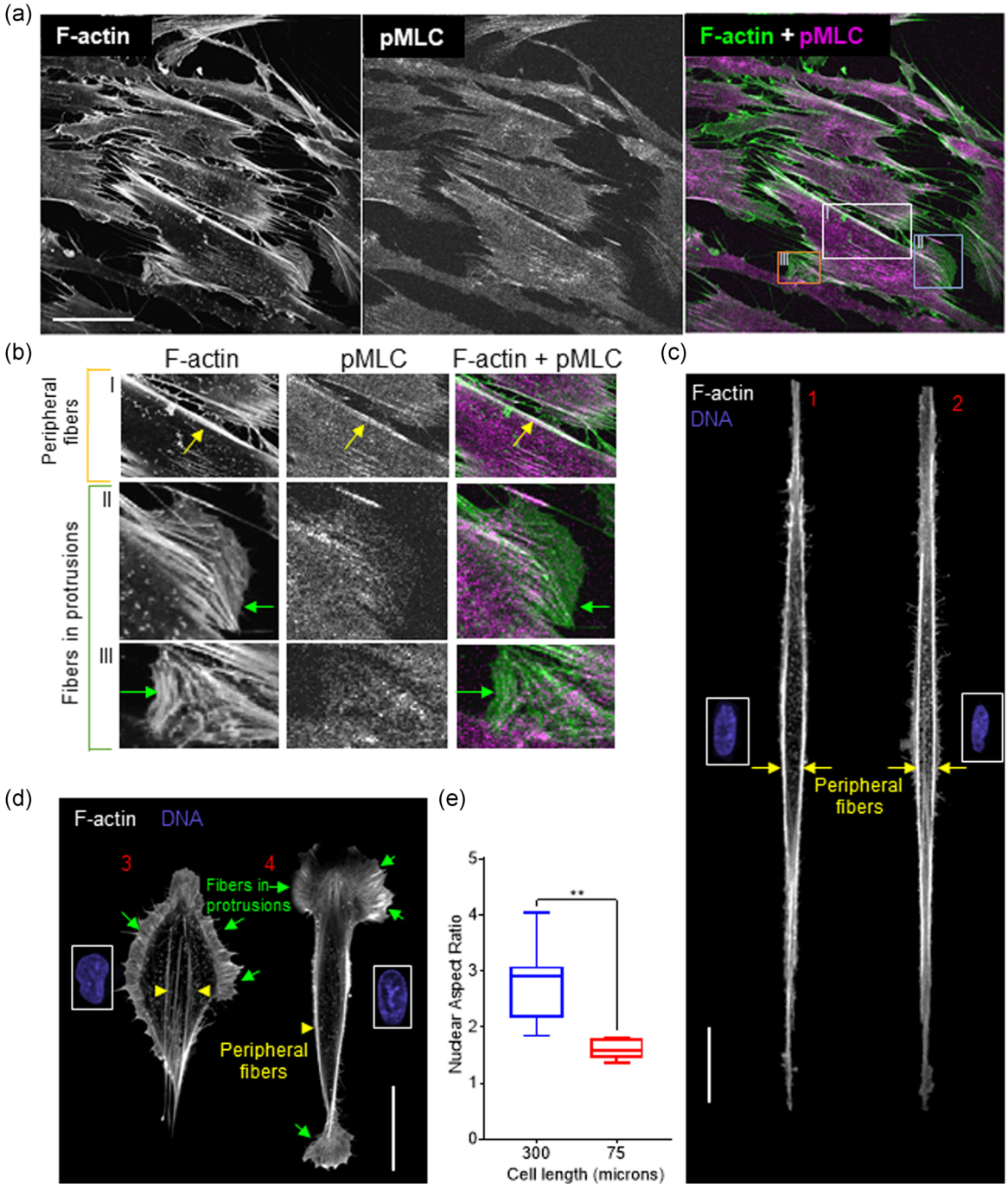

FIGURE 2 Nuclear morphology and F-actin fiber distribution in cultured PdLFs. (a) Fixed PdLFs stained for F-actin and phosphorylated nonmuscle myosin light chain-II (pMLC). Scale bar is 50 μm. Insets in (b) show regions of colocalization of F-actin and pMLC (yellow arrows) and regions of noncolocalization (green arrows). PdLFs fixed and stained for F-actin and DNA cultured on micro-contact printed 1-D lines (c) 300 μm in length (Scale bar is 30 μm), and (d) 75 μm in length (Scale bar is 25 μm) are shown. Yellow arrows mark contractile fibers and green arrows mark non-contractile fibers. (e) Comparison of nuclear aspect ratio of cells micropatterned on on 300 micron (n = 10 cells) and 75 micron (n = 7 cells) 1-D lines. "**" Represents statistically significant difference by Mann–Whitney test (p = .0025). PdLF, periodontal ligament fibroblast

evidence that tensile stress or compressive stress altered the levels of these molecules. We chose to measure the levels of the osteoclastogenesis-inhibitory molecule OPG, and matrix metalloproteinases MMP-2 and MMP-3. OPG levels in PdLFs are sensitive to externally applied mechanical stress (Kook et al., 2009). Likewise, mechanical stress has been observed to alter MMPs expression in PdLFs (He et al., 2004). Receptor activator for nuclear factor κB ligand (RANKL), which promotes osteoclastogenesis, was found to be negligibly expressed in cultured PdLFs under all conditions and was therefore not included in the analysis.

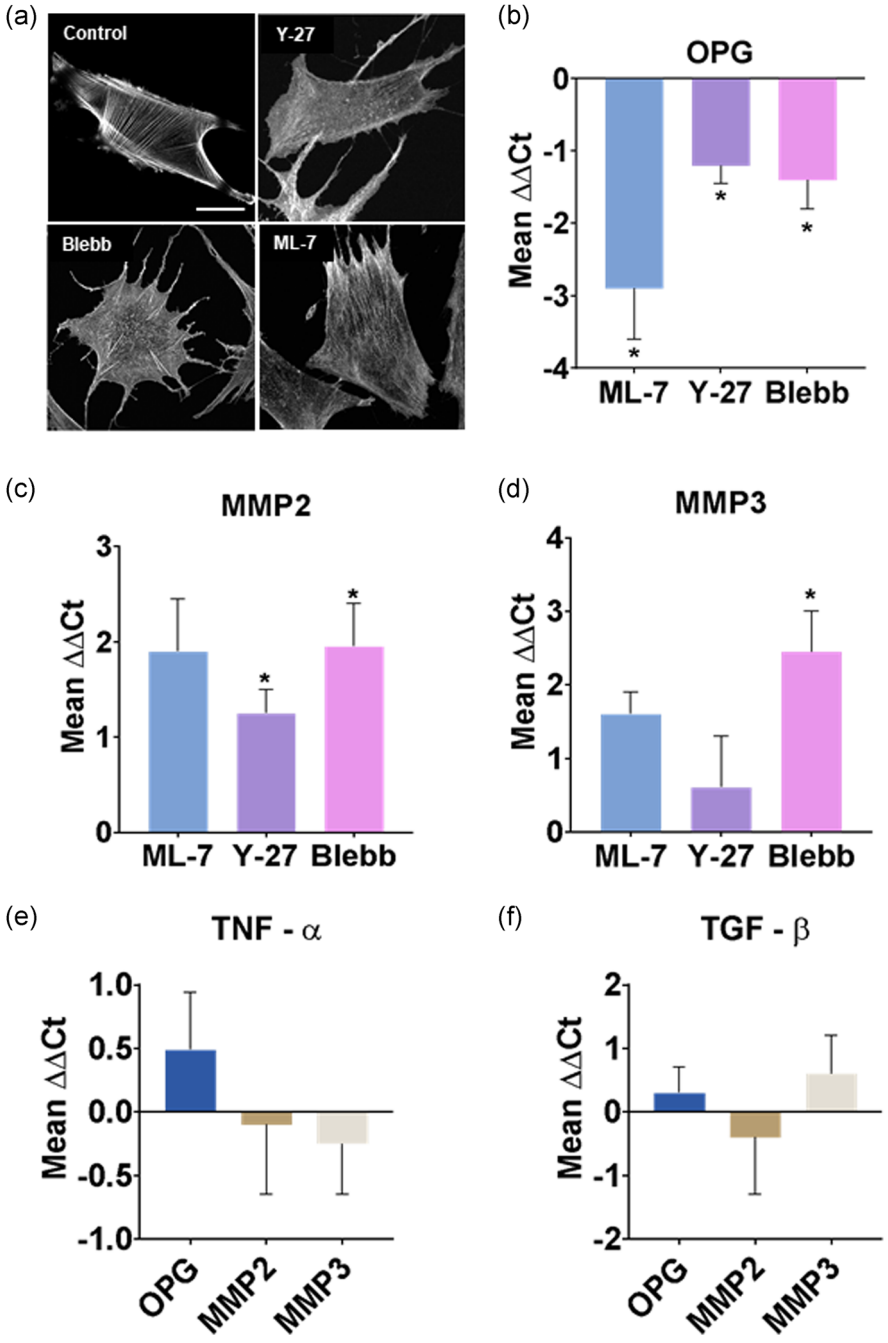

FIGURE 3 Effect of inhibitors on F-actin fiber assembly and mRNA levels of chosen genes. (a) F-actin images of PdLFs post drug-treatment for 24 h: control (DMSO), Y-27 (10 μM), Blebbistatin (30 μM) and ML-7 (40 μM). Scale bar is 20 μm. Graphs show effect of inhibitors on mean ΔΔCt, the log-fold change in mRNA levels of OPG (b), MMP-2 (c) and MMP-3 (d), each relative to DMSO treatment. Error bars are *SEM*. *Indicates $p < .05$ by Welch *t* test with Benjamini-Hochberg corrections for multiple comparisons. (e, f) Graphs show corresponding mean ΔΔCt for the same genes upon treatment with TNF-α or TGF-β, respectively, relative to DMSO control. Error bars are *SEM*. DMSO, dimethyl sulfoxide; mRNA, messenger RNA; OPG, osteoprotegerin; PdLF, periodontal ligament fibroblast; TGF-β, transforming growth factor beta; TNF-α, tumor necrosis factor-alpha

mRNA levels corresponding to these three genes were quantified using RT-qPCR. The ΔCt values were calculated relative to the levels of GAPDH, and statistically compared with the DMSO control using an unpaired Welch's *t* test with Benjamini Hochberg corrections whenever there were multiple comparisons (Reiner et al., 2003; Wang et al., 2006; Yuan et al., 2006). Statistically significant changes in ΔCt values are indicated in Figure 3d which shows a plot of mean values of ΔΔCt, the log-fold change in mRNA levels relative to the control treated with vehicle (DMSO). Each of the three myosin inhibitors significantly reduced the levels of OPG relative to the DMSO control (Figure 3b). The consistent

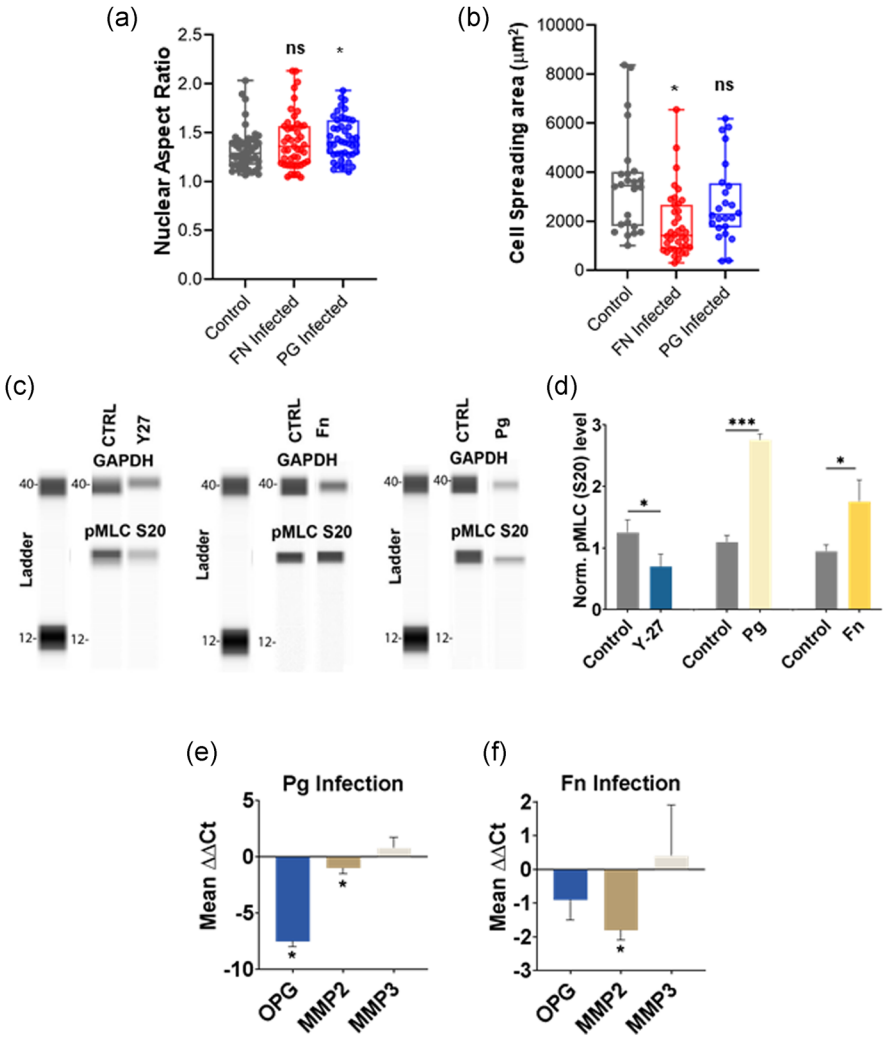

FIGURE 4 Effect of *P. gingivalis* or *F. nucleatum* infection on pMLC levels and mRNA levels in PdLFs. (a, b) Nuclear aspect ratio and spreading area of cells after bacterial infection for 24 h. $n > 45$ for nuclear measurements, and $n > 24$ for cell spreading area measurements. Statistical significance with respect to control was determined by Kruskal–Wallis test with Dunn's multiple comparison, $^{*}p < .05$, ns: $p > .05$. (c) The western blots acquired with the simple Wes system (see Section 2) of pMLC levels assayed in lysates from PdLF cells with antimyosin light chain (phospho S20) antibody. Pg: *P. gingivalis* infection of PdLF cells for 24 h; Fn: *F. nucleatum* infection of PdLF cells for 24 h; Y27: 25 μM Y27632 treatment for 24 h; DMSO was included as vehicle control. (d) Graph shows normalized pMLC levels corresponding to the data in (c). Error bars indicate ± *SEM* ($^{*,**,***}p < .05$ by Welch *t* test for statistical comparisons with Benjamini-Hochberg corrections for multiple comparisons). (e, f) Graph shows mean ΔΔCt, the log-fold change in mRNA levels of OPG, MMP-2 and MMP-3 in infected PdLFs relative to DMSO treatment. *Indicates $p < .05$ by Welch *t* test with Benjamini-Hochberg corrections for multiple comparisons. DMSO, dimethyl sulfoxide; mRNA, messenger RNA; MMP, matrix metalloproteinases; PdLF, periodontal ligament fibroblast

response of OPG levels to modulation of actomyosin contractility by three different pharmacological drugs leads us to conclude that OPG levels are mechano-sensitive to PdLF actomyosin tension.

In contrast, MMP-2 and MMP-3 mRNA levels were affected inconsistently by the different myosin inhibitors (Figure 3c,d). Treatment of cells with Y27632 and blebbistatin increased MMP2 levels while ML-7 treatment had no effect. Blebbistatin treatment decreased MMP3 levels, but ML-7 and Y27632 had no effect. Finally, treatment with TNF-α or TGF-β (both at 5 ng/ml for 24 h) did not cause any measurable changes in OPG, MMP3, or MMP2 levels (Figure 3e,f). Collectively these results further support our finding that NMMII generated tension is a potent regulator of OPG gene expression.

3.4 | In vitro bacterial infection for 24 h does not capture phenotypic effects observed in vivo

Previous studies have shown that bacterial infection decreases OPG levels in PdLFs (Belibasakis et al., 2007; Crotti et al., 2003). Given the mechanosensitivity of OPG observed above, we hypothesized that pMLC levels would decrease upon infection by *P. gingivalis* or *F. nucleatum*, two different species implicated in periodontal disease. After infection for 24 h with *P. gingivalis* and *F. nucleatum* (MOI: 100), we quantified nuclear phenotypes in infected cells. Nuclear aspect ratio was unaffected by *P. gingivalis* infection while it actually increased relative to control upon

F. nucleatum infection (Figure 4a). Cell spreading was reduced somewhat upon *F. nucleatum* infection and was unaffected upon *P. gingivalis* infection (Figure 4b). Thus, the in vitro infection assay fails to capture the morphological effects of infection on cells observed in vivo.

We next measured the effect of infection on pMLC levels in PdLFs with western blotting. We confirmed that Y27 treatment had the desired effect of reduction in pMLC levels (Zhang et al., 2019; Figure 4c). Infection with *P. gingivalis* or *F. nucleatum* resulted in an increase in pMLC levels as measured with western blotting (Figure 4c,d). We next quantified the levels of OPG, MMP-2, and MMP-3 in infected cells. Infection by *P. gingivalis* reduced the mRNA levels of OPG (Figure 4e), while *F. nucleatum* decreased them without reaching statistical significance (Figure 4f). Infection with either bacterium had no effect on MMP-3 levels, while both bacteria caused a reduction in MMP-2 levels (Figure 4e,f).

4 | DISCUSSION

The PDL, cementum and alveolar bone are all load-bearing complexes which are likely impacted in PD. Here we showed using a mouse model of PD that the nucleus is rounded and loses its orientation in the PDL upon infection for many weeks with a cocktail of bacteria. We interpret the nuclear rounding and loss of orientation as suggestive of a rounding of the PdLFs and a decrease in actomyosin contractility upon infection. Consistent with our interpretation, our in vitro studies showed that rounded PdLFs have rounded nuclei, while elongated PdLFs have elongated nuclei. Further, elongated PdLFs have F-actin fiber distributions consistent with higher contractility compared with rounded PdLFs. Collectively, our in vitro and in vivo findings suggest a potential role for reduced PdLF actomyosin tension in the progression of periodontal disease.

We took the next logical step of inhibiting actomyosin contractility in cultured PdLFs and quantifying OPG levels. OPG levels in PdLFs were decreased upon decreasing actomyosin tension (Figure 3), as evidenced by their consistent changes under treatment with three different inhibitors which ultimately reduce actomyosin contractility. MMP levels, on the other hand, were not consistently affected by drug treatments. Our results suggest that OPG mechanosensitivity is likely regulated by the RhoA pathway; unraveling these pathways will help understand the relationship between OPG and actomyosin tension.

Our in vitro experiments involving infection of primary human PdLFs with bacteria for 24 h failed to capture the phenotypic effects, specifically nuclear rounding, observed in the mouse model. A key difference is the fact that cultured PdLFs do not have the highly elongated morphologies characteristic of PdLFs in vivo. Also, it is unclear if bacteria infect PdLFs directly in vivo, or whether toxins secreted by bacterial biofilms elsewhere in the periodontium indirectly affect PdLF morphology. The in vitro assay also features a much shorter time of infection compared to the 16-week infection protocol for our mouse model.

While our in vitro experiments are disappointingly (but not surprisingly) inapplicable to the in vivo situation, it is still useful to analyze the observed increase in pMLC levels upon bacterial infection on pMLC levels. The fact that OPG is reduced upon bacterial infection suggests the existence of pathways that over-ride OPG's mechanosensitivity to actomyosin contractility. Alternatively, bacterial infection could reverse the direction of mechanosensitivity in PdLFs, given that OPG reduces in levels upon bacterial infection. Reversal of the direction of gene mechanosensitivity (as opposed to loss of mechanosensitivity) is not entirely unexpected as it has been reported in other contexts (Alam et al., 2016). Consistent with the notion of abnormal mechanosensitivity, PdLFs from periodontal tissue infected with bacteria display pathologic responses to external mechanical stresses by expressing inflammatory cytokines, matrix metalloproteinases and osteoclastic molecules (El-Awady et al., 2010a; Sokos et al., 2015a).

That infection by two distinct periodontal bacteria consistently increase NMMII phosphorylation in PdLFs in culture are in line with other studies that infection of *P. gingivalis* into gingival epithelial cells increases assembly of integrin-associated focal adhesions with subsequent remodeling of the F-actin and microtubule cytoskeleton (Yilmaz et al., 2002). Likewise, it is well known that NMMII or other myosin isoforms are important in bacterial infection of other cell types. For example, pathogenic bacteria like *Shigella flexneri* use NMMII for dissemination from cell to cell in infected Caco-2 cells (Rathman et al., 2000). Different myosin isoforms including NMMII are recruited to the phagocytic cup in macrophages and help in internalization of target (Rougerie et al., 2013).

Our results highlight the need to understand the molecular mechanisms by which PDLF nuclear shape and actomyosin contractility are impacted in vivo and in vitro by bacterial infection, and their relationship with bone regulatory gene expression. We predict that this may help develop new therapeutic strategies for long-term maintenance of the periodontium during PD.

ACKNOWLEDGMENTS

Tanmay P. Lele acknowledges support from the CPRIT established investigator (award no.: #RR200043). Pankaj K. Singh is supported via the CPRIT-funded the Combinatorial Drug Discovery Program (CDDP) (RP200668). Sasanka S. Chukkapalli acknowledges support from the Center for Molecular Microbiology, University of Florida, Gainesville.

CONFLICT OF INTERESTS

The authors declare that there are no conflict of interests.

AUTHOR CONTRIBUTIONS

Tanmay Lele and Sasanka Chukkapalli designed the research plan. Andrew Tamashunas, Aditya Katiyar, Qiao Zhang, Purboja Purkayastha, and Sasanka Chukkapalli performed the experiments and collected data. All authors contributed to analyzing data. Tanmay Lele wrote the manuscript with input from all authors, and Aditya Katiyar prepared the figures with input from all authors.

DATA AVAILABILITY STATEMENT

The data that support the findings of this study are available from the corresponding author upon reasonable request.

ORCID

Qiao Zhang http://orcid.org/0000-0003-1374-1898
Sasanka S. Chukkapalli http://orcid.org/0000-0001-9063-6907

REFERENCES

Alam, S., Zhang, Q., Prasad, N., Li, Y., Chamala, S., Kuchibhotla, R., Aggarwal, V., Shrestha, S., Jones, A., Levy, S., Roux, K., Nickerson, J., & Lele, T. (2016). The mammalian LINC complex regulates genome transcriptional responses to substrate rigidity. *Scientific Reports*, *6*, 38063.

Assis Lisboa, R., Lisboa, F., Santos, G., Andrade, M., & Cunha-Melo, J. (2009). Matrix metalloproteinase 2 activity decreases in human periodontal ligament fibroblast cultures submitted to simulated orthodontic force. *In Vitro Cellular & Developmental Biology. Animal*, *45*, 614–621.

Balaban, N. Q., Schwarz, U. S., Riveline, D., Goichberg, P., Tzur, G., Sabanay, I., Mahalu, D., Safran, S., Bershadsky, A., Addadi, L., & Geiger, B. (2001). Force and focal adhesion assembly: A close relationship studied using elastic micropatterned substrates. *Nature Cell Biology*, *3*, 466–472.

Beach, J. R., Shao, L., Remmert, K., Li, D., Betzig, E., & Hammer, J. A., 3rd. (2014). Nonmuscle myosin II isoforms coassemble in living cells. *Current Biology*, *24*, 1160–1166.

Belibasakis, G. N., Bostanci, N., Hashim, A., Johansson, A., Aduse-Opoku, J., Curtis, M. A., & Hughes, F. J. (2007). Regulation of RANKL and OPG gene expression in human gingival fibroblasts and periodontal ligament cells by *Porphyromonas gingivalis:* A putative role of the Arg-gingipains. *Microbial Pathogenesis*, *43*, 46–53.

Berkovitz, B. K. (1990). The structure of the periodontal ligament: An update. *European Journal of Orthodontics*, *12*, 51–76.

Binderman, I., Bahar, H., & Yaffe, A. (2002). Strain relaxation of fibroblasts in the marginal periodontium is the common trigger for alveolar bone resorption: A novel hypothesis. *Journal of Periodontology*, *73*, 1210–1215.

Binderman, I., Gadban, N., & Yaffe, A. (2014). Cytoskeletal disease: A role in the etiology of adult periodontitis. *Oral Diseases*, *20*, 10–16.

Bruyère, C., Versaevel, M., Mohammed, D., Alaimo, L., Luciano, M., Vercruysse, E., & Gabriele, S. (2019). Actomyosin contractility scales with myoblast elongation and enhances differentiation through YAP nuclear export. *Scientific Reports*, *9*, 15565.

Cekici, A., Kantarci, A., Hasturk, H., & Van Dyke, T. E. (2014). Inflammatory and immune pathways in the pathogenesis of periodontal disease. *Periodontology 2000*, *64*, 57–80.

Chen, C. S., Alonso, J. L., Ostuni, E., Whitesides, G. M., & Ingber, D. E. (2003). Cell shape provides global control of focal adhesion assembly. *Biochemical and Biophysical Research Communications*, *307*, 355–361.

Chicurel, M. E., Chen, C. S., & Ingber, D. E. (1998). Cellular control lies in the balance of forces. *Current Opinion in Cell Biology*, *10*, 232–239.

Chukkapalli, S. S., & Lele, T. P. (2018). Periodontal cell mechanotransduction. *Open Biology*, *8*, 180053.

Chukkapalli, S., Rivera-Kweh, M., Gehlot, P., Velsko, I., Bhattacharyya, I., Calise, S. J., Satoh, M., Chan, E. K. L., Holoshitz, J., & Kesavalu, L. (2016). Periodontal bacterial colonization in synovial tissues exacerbates collagen-induced arthritis in B10.RIII mice. *Arthritis Research & Therapy*, *18*, 161.

Chukkapalli, S. S., Velsko, I. M., Rivera-Kweh, M. F., Zheng, D., Lucas, A. R., & Kesavalu, L. (2015). Polymicrobial oral infection with four periodontal bacteria orchestrates a distinct inflammatory response and atherosclerosis in ApoE null mice. *PLoS One*, *10*, e0143291.

Crotti, T., Smith, M. D., Hirsch, R., Soukoulis, S., Weedon, H., Capone, M., Ahern, M. J., & Haynes, D. (2003). Receptor activator NF kappaB ligand (RANKL) and osteoprotegerin (OPG) protein expression in periodontitis. *Journal of Periodontal Research*, *38*, 380–387.

El-Awady, A. R., Messer, R. L., Gamal, A. Y., Sharawy, M. M., Wenger, K. H., & Lapp, C. A. (2010a). Periodontal ligament fibroblasts sustain destructive immune modulators of chronic periodontitis. *Journal of Periodontology*, *81*, 1324–1335.

El-Awady, A. R., Messer, R. L. W., Gamal, A. Y., Sharawy, M. M., Wenger, K. H., & Lapp, C. A. (2010b). Periodontal ligament fibroblasts sustain destructive immune modulators of chronic periodontitis. *Journal of Periodontology*, *81*, 1324–1335.

Goffin, J. M., Pittet, P., Csucs, G., Lussi, J. W., Meister, J. J., & Hinz, B. (2006). Focal adhesion size controls tension-dependent recruitment of alpha-smooth muscle actin to stress fibers. *Journal of Cell Biology*, *172*, 259–268.

He, Y., Macarak, E. J., Korostoff, J. M., & Howard, P. S. (2004). Compression and tension: Differential effects on matrix accumulation by periodontal ligament fibroblasts in vitro. *Connective Tissue Research*, *45*, 28–39.

Hyun, S. Y., Lee, J. H., Kang, K. J., & Jang, Y. J. (2017). Effect of FGF-2, TGF-beta-1, and BMPs on teno/ligamentogenesis and osteo/cementogenesis of human periodontal ligament stem cells. *Molecules and Cells*, *40*, 550–557.

Ingber, D. E., Prusty, D., Sun, Z., Betensky, H., & Wang, N. (1995). Cell shape, cytoskeletal mechanics, and cell cycle control in angiogenesis. *Journal of Biomechanics*, *28*, 1471–1484.

Jang, A. T., Chen, L., Shimotake, A. R., Landis, W., Altoe, V., Aloni, S., Ryder, M., & Ho, S. P. (2018). A force on the crown and tug of war in the periodontal complex. *Journal of Dental Research*, *97*, 241–250.

Jiao, Y., Hasegawa, M., & Inohara, N. (2014). The role of oral pathobionts in dysbiosis during periodontitis development. *Journal of Dental Research*, *93(6)*, 539–546.

Kassianidou, E., & Kumar, S. (2015). A biomechanical perspective on stress fiber structure and function. *Biochimica et Biophysica Acta/General Subjects*, *1853*, 3065–3074.

Katiyar, A., Tocco, V. J., Li, Y., Aggarwal, V., Tamashunas, A. C., Dickinson, R. B., & Lele, T. P. (2019). Nuclear size changes caused by local motion of cell boundaries unfold the nuclear lamina and dilate chromatin and intranuclear bodies. *Soft Matter*, *15*, 9310–9317.

Katoh, K., Kano, Y., Amano, M., Kaibuchi, K., & Fujiwara, K. (2001). Stress fiber organization regulated by MLCK and Rho-kinase in cultured human fibroblasts. *American Journal of Physiology: Cell Physiology*, *280*, C1669–C1679.

Kim, T., Handa, A., Iida, J., & Yoshida, S. (2007). RANKL expression in rat periodontal ligament subjected to a continuous orthodontic force. *Archives of Oral Biology*, *52*, 244–250.

Konermann, A., Stabenow, D., Knolle, P. A., Held, S. A., Deschner, J., & Jager, A. (2012). Regulatory role of periodontal ligament fibroblasts for innate immune cell function and differentiation. *Innate Immunity*, *18*, 745–752.

Kook, Y. A., Lee, S. K., Son, D. H., Kim, Y., Kang, K. H., Cho, J. H., Kim, S. C., Kim, Y. S., Lee, H. J., Lee, S. K., & Kim, E. C. (2009). Effects of substance P on osteoblastic differentiation and heme oxygenase-1 in human periodontal ligament cells. *Cell Biology International*, *33*, 424–428.

Kumar, S., Maxwell, I. Z., Heisterkamp, A., Polte, T. R., Lele, T. P., Salanga, M., Mazur, E., & Ingber, D. E. (2006). Viscoelastic retraction of single living stress fibers and its impact on cell shape, cytoskeletal organization, and extracellular matrix mechanics. *Biophysical Journal*, *90*, 3762–3773.

Lamont, R. J., & Hajishengallis, G. (2015). Polymicrobial synergy and dysbiosis in inflammatory disease. *Trends in Molecular Medicine*, *21(3)*, 172–183.

Lee, S., & Kumar, S. (2016). Actomyosin stress fiber mechanosensing in 2D and 3D. *F1000Research*, *5*, 2261.

Lee, J. H., Pryce, B. A., Schweitzer, R., Ryder, M. I., & Ho, S. P. (2015). Differentiating zones at periodontal ligament-bone and periodontal ligament-cementum entheses. *Journal of Periodontal Research*, *50*, 870–880.

Lele, T. P., Dickinson, R. B., & Gundersen, G. G. (2018). Mechanical principles of nuclear shaping and positioning. *Journal of Cell Biology*, *217*, 3330–3342.

Lele, T. P., Pendse, J., Kumar, S., Salanga, M., Karavitis, J., & Ingber, D. E. (2006). Mechanical forces alter zyxin unbinding kinetics within focal adhesions of living cells. *Journal of Cellular Physiology*, *207*, 187–194.

Liu, M., Dai, J., Lin, Y., Yang, L., Dong, H., Li, Y., Ding, Y., & Duan, Y. (2012). Effect of the cyclic stretch on the expression of osteogenesis genes in human periodontal ligament cells. *Gene*, *491*, 187–193.

Luo, Y. H., Ouyang, P. B., Tian, J., Guo, X. J., & Duan, X. C. (2014). Rosiglitazone inhibits TGF-beta 1 induced activation of human Tenon fibroblasts via p38 signal pathway. *PLoS One*, *9*, e105796.

Mammoto, T., Mammoto, A., & Ingber, D. E. (2013). Mechanobiology and developmental control. *Annual Review of Cell and Developmental Biology*, *29*, 27–61.

Marsh, P. D. (2015). The commensal microbiota and the development of human disease—An introduction. *Journal of Oral Microbiology*, *7*, 29128.

McCulloch, C. A., Lekic, P., & McKee, M. D. (2000). Role of physical forces in regulating the form and function of the periodontal ligament. *Periodontology 2000*, *24*, 56–72.

Moore, W. E. C., & Moore, L. V. H. (1994). The bacteria of periodontal diseases. *Periodontology 2000*, *5(1)*, 66–77.

Palioto, D. B., Rodrigues, T. L., Marchesan, J. T., Beloti, M. M., de Oliveira, P. T., & Rosa, A. L. (2011). Effects of enamel matrix derivative and transforming growth factor-beta1 on human osteoblastic cells. *Head & Face Medicine*, *7*, 13.

Pihlstrom, B. L., Michalowicz, B. S., & Johnson, N. W. (2005). Periodontal diseases. *The Lancet*. *366*, 1809–1820.

Polte, T. R., Eichler, G. S., Wang, N., & Ingber, D. E. (2004). Extracellular matrix controls myosin light chain phosphorylation and cell contractility through modulation of cell shape and cytoskeletal prestress. *American Journal of Physiology: Cell Physiology*, *286*, C518–C528.

Prager-Khoutorsky, M., Lichtenstein, A., Krishnan, R., Rajendran, K., Mayo, A., Kam, Z., Geiger, B., & Bershadsky, A. D. (2011). Fibroblast polarization is a matrix-rigidity-dependent process controlled by focal adhesion mechanosensing. *Nature Cell Biology*, *13*, 1457–1465.

Rathman, M., de Lanerolle, P., Ohayon, H., Gounon, P., & Sansonetti, P. (2000). Myosin light chain kinase plays an essential role in S. flexneri dissemination. *Journal of Cell Science*, *113*(Pt 19), 3375–3386.

Reiner, A., Yekutieli, D., & Benjamini, Y. (2003). Identifying differentially expressed genes using false discovery rate controlling procedures. *Bioinformatics*, *19*, 368–375.

Ridley, A. J., & Hall, A. (1992). Distinct patterns of actin organization regulated by the small GTP-binding proteins Rac and Rho. *Cold Spring Harbor Symposia on Quantitative Biology*, *57*, 661–671.

Ridley, A. J., & Hall, A. (1994). Signal transduction pathways regulating Rho-mediated stress fibre formation: Requirement for a tyrosine kinase. *EMBO Journal*, *13*, 2600–2610.

Roberts, F. A., & Darveau, R. P. (2015). Microbial protection and virulence in periodontal tissue as a function of polymicrobial communities: Symbiosis and dysbiosis. *Periodontology 2000*, *69*, 18–27.

Rougerie, P., Miskolci, V., & Cox, D. (2013). Generation of membrane structures during phagocytosis and chemotaxis of macrophages: Role and regulation of the actin cytoskeleton. *Immunological Reviews*, *256*, 222–239.

Russell, R. J., Xia, S. L., Dickinson, R. B., & Lele, T. P. (2009). Sarcomere mechanics in capillary endothelial cells. *Biophysical Journal*, *97*, 1578–1585.

Socransky, S. S., & Haffajee, A. D. (2005). Periodontal microbial ecology. *Periodontology 2000*, *38*, 135–187.

Sokos, D., Everts, V., & de Vries, T. J. (2015a). Role of periodontal ligament fibroblasts in osteoclastogenesis: A review. *Journal of Periodontal Research*, *50*, 152–159.

Sokos, D., Everts, V., & de Vries, T. J. (2015b). Role of periodontal ligament fibroblasts in osteoclastogenesis: A review. *Journal of Periodontal Research*, *50*, 152–159.

Stachowiak, M. R., & O'Shaughnessy, B. (2009). Recoil after severing reveals stress fiber contraction mechanisms. *Biophysical Journal*, *97*, 462–471.

Tanner, K., Boudreau, A., Bissell, M. J., & Kumar, S. (2010). Dissecting regional variations in stress fiber mechanics in living cells with laser nanosurgery. *Biophysical Journal*, *99*, 2775–2783.

Thery, M., & Piel, M. (2009). Adhesive micropatterns for cells: A microcontact printing protocol. *Cold Spring Harbor Protocols*, *2009*, pdb.prot5255.

Tomasek, J. J., Haaksma, C. J., Schwartz, R. J., & Howard, E. W. (2013). Whole animal knockout of smooth muscle alpha-actin does not alter excisional wound healing or the fibroblast-to-myofibroblast transition. *Wound Repair and Regeneration*, *21*, 166–176.

Tsuji, K., Uno, K., Zhang, G. X., & Tamura, M. (2004). Periodontal ligament cells under intermittent tensile stress regulate mRNA expression of osteoprotegerin and tissue inhibitor of matrix metalloprotease-1 and -2. *Journal of Bone and Mineral Metabolism*, *22*, 94–103.

Wang, Y., Joshi, T., Zhang, X., Xu, D., & Chen, L. (2006). Inferring gene regulatory networks from multiple microarray datasets. *Bioinformatics (Oxford, England)*, *22*, 2413–2420.

Wipff, P. J., Rifkin, D. B., Meister, J. J., & Hinz, B. (2007). Myofibroblast contraction activates latent TGF-beta1 from the extracellular matrix. *Journal of Cell Biology*, *179*, 1311–1323.

Yilmaz, O., Watanabe, K., & Lamont, R. J. (2002). Involvement of integrins in fimbriae-mediated binding and invasion by Porphyromonas gingivalis. *Cellular Microbiology*, *4*, 305–314.

Yuan, J. S., Reed, A., Chen, F., & Stewart, C. N., Jr. (2006). Statistical analysis of real-time PCR data. *BMC Bioinformatics*, *7*, 85.

Zhang, Q., Narayanan, V., Mui, K. L., O'Bryan, C. S., Anderson, R. H., Kc, B., Cabe, J. I., Denis, K. B., Antoku, S., Roux, K. J., Dickinson, R. B., Angelini, T. E., Gundersen, G. G., Conway, D. E., & Lele, T. P. (2019). Mechanical stabilization of the glandular acinus by linker of nucleoskeleton and cytoskeleton complex. *Current Biology*, *29*, 2826–2839.

Ziegler, N., Alonso, A., Steinberg, T., Woodnutt, D., Kohl, A., Müssig, E., Schulz, S., & Tomakidi, P. (2010). Mechano-transduction in periodontal ligament cells identifies activated states of MAP-kinases p42/44 and p38-stress kinase as a mechanism for MMP-13 expression. *BMC Cell Biology*, *11*, 10.

SUPPORTING INFORMATION

Additional Supporting Information may be found online in the supporting information tab for this article.

How to cite this article: Tamashunas AC, Katiyar A, Zhang Q, et al. Osteoprotegerin is sensitive to actomyosin tension in human periodontal ligament fibroblasts. *J Cell Physiol*. 2021;1–11. https://doi.org/10.1002/jcp.30256